Assessment of human health impact from exposure to multiple air pollutants in China based on satellite observations

Tao Yu [a,b,c], Wen Wang [a, *], Pubu Ciren [a,d], Yan Zhu [a],

a Center for Spatial Information, School of Environment and Natural Resources, Renmin University of China, Beijing 100872, China

b State Key Laboratory of Remote Sensing Science, Jointly Sponsored by Beijing Normal University and the Institute of Remote Sensing Applications, CAS, Beijing 100875, China

c School of Geography and Remote Sensing Sciences, Beijing Normal University, Beijing 100875, China

d IMSG at NOAA/NESDIS/STAR, 5825 University Research Center, , Maryland 20740, USA

*****Corresponding author. Tel.: +86-10-8889-3061. Email: wen_wang2000@hotmail.com (W. Wang)

Email addresses: yutaogis@hotmail.com (T. Yu), pubu.ciren@noaa.gov (P. Ciren), zhuyan@ruc.edu.cn (Y. Zhu)

Assessment of human health impact from exposure to multiple air pollutants in China based on satellite observations

Abstract

Assessment of human health impact caused by air pollution is crucial for evaluating environmental hazards. In this paper, concentrations of six air pollutants (PM_{10}, $PM_{2.5}$, NO_2, SO_2, O_3, and CO) were first derived from satellite observations, and then the overall human health risks in China caused by multiple air pollutants were assessed using an aggregated health risks index. Unlike traditional approach for human health risks assessment, which relied on the in-situ air pollution measurements, the spatial distribution of aggregated human health risks in China were obtained using satellite observations in this research. It was indicated that the remote sensing data have advantages over in-situ data in accessing human health impact caused by air pollution.

Key words: multiple air pollutants; human health; assessment; distribution; remote sensing

1 Introduction

Air pollution is a significant health hazard worldwide. Studies have shown that air pollution attributed to about 1.2% of annual total deaths globally (Chen et al., 2005), and accounted for more than two million premature deaths each year (WHO, 2005). Among these air pollution related deaths, nearly half of them occurred in developing countries (WHO, 2005). In China, air pollution causes more than one million premature deaths and 76 million disability-adjusted life years every year, and the corresponding disease burden increased by 33% in past 20 years (Murray et al., 2013). Moreover, with the accelerating industrialization, air pollution in China has been becoming a serious regional environmental issue, which not only endangered human health, but also restricted economic development (Chan and Yao, 2008). Therefore, studies on the human health impact caused by air pollution in China are of great significance in

providing more detailed information for evaluating environmental damages.

In many previous studies, assessing the impact of air pollutants on human health relied typically on in-situ measurements of air pollution. These studies usually used observations over air pollution monitoring stations to find the relationship between human health and the exposure to particulate matter (PM) (Janssen et al., 2002; Brauer et al.,2003; Putaud et al., 2010; Turner et al., 2011), nitrogen dioxides (Wheeler et al., 2008; Raaschou-Nielsen et al., 2013), sulfur dioxide (Kan et al., 2010; Chen et al., 2012), carbon dioxide (Raub et al., 2000; Bernstein et al., 2004) and ozone (Wang et al., 2003; Jerrett et al., 2009). However, it is well known that air pollution monitoring stations are usually located in areas where air pollution is serious, hence, using the ground based monitoring data alone is likely to misrepresent the regional concentrations of air pollutants and leads to overestimate human health impact as a result of the high-biased regional air pollutants concentrations from solely in-situ measurements. Although some interpolation methods have been applied to calculate concentrations of air pollutants from measurements over the irregularly distributed stations in epidemiological studies (Jerrett et al., 2005; Smith et al., 2010; Lipsett et al., 2011), these methods are constrained by physiochemical models and may not give physically consistent results, especially over areas with complex terrain (Hertel et al., 2001). In addition, previous studies mainly focused on human health impact from a single pollutant (Brauer et al.,2003; Wheeler et al., 2008；Anderson et al, 2012; Dergham et al., 2015), which is inadequate to reflect overall air pollution damages to human health.

To account for the realistic spatial variability of air pollutants, we used the technology of remote sensing in this research. Remote sensing is the science of obtaining the information about objects or areas, typically from aircrafts or satellites. The technology of remote sensing has a wide range of applications in many different fields, due to its advantages in large spatial and temporal coverage (Campbell, 2002). In this paper, concentrations of air pollutants were derived from remote sensing data. Therefore, concentrations of air pollutants over areas with no ground observations are

also available. To link air pollution and corresponding human health impact, we first obtained the spatial distribution of human health risks related to individual pollutant, and then an aggregated human health risks index is used to access the overall impact by exposure to multiple air pollutants. This index reflects the combined health impact from various air pollutants by linking concentrations of each individual air pollutant with the human mortality to determine the contribution of each air pollutant to human health. Concentrations of five air pollutants, i.e., PM_{10}, $PM_{2.5}$, NO_2, SO_2, O_3 and CO, and their corresponding human health risks are included in this index.

In this paper, concentrations of five air pollutants were first calculated with satellite observations, i.e., concentrations of PM_{10}、 $PM_{2.5}$ were derived from ozone monitoring instrument (OMI) Aerosol Optical Depth (AOD) product, concentrations of SO_2, NO_2 andO_3 were derived from OMI Level-2 product, and concentrations of CO were derived from SCIAMACHY Level-2 product. Secondly, human health risks of these five air pollutants were then evaluated with an aggregated risks index (ARI), and the spatial distribution of the ARI was analyzed. Finally, the derived concentrations of these five air pollutants from satellite observations were validated with the ground-based measurements, and the advantages of using satellite observations in accessing human health risk from air pollutants were discussed.

2 Data and methods

2.1 Study area

China is located in the east of Asia and the west of Pacific, its climate is significantly affected by both continent and ocean. It blows mainly southeast winds in summer and northwest winds in winter (Ding et al., 1995). With the rapid process of industrialization, air pollution has become one of the top environmental concerns in China (Chan and Yao, 2008). Coal dominated energy and the increasing number of motor vehicles have led to the deterioration of air quality. More serious air pollution has been developed over cities and industrial zones as a result of overlaying of different

types of air pollutants. The studies by World Bank have shown that, among the largest 500 cities in China, only 1% of them are able to reach the air quality standards recommended by World Health Organization (WHO), and seven Chinese cities were listed in the top ten most polluted cities in the world (Zhang and Crooks, 2013). Although the Chinese government has been actively taking financial and administrative measures to combat air pollution, air pollution control in China still face huge challenges and tremendous pressure.

2.2 Methods

2.2.1 Aggregate health risks index

Particular matters, sulfur dioxide, nitrogen oxide, ozone and carbon monoxide, which pose the biggest threat to human beings, are the major air pollutants observed in China (Chen et al., 2004). The studies on the exposure-response relationships and human health endpoints in China have also indicated the associations with these air pollutants (Shang et al., 2013). Therefore, PM_{10}, $PM_{2.5}$, NO2, SO_2, O_3 and CO was selected as the major air pollutants to assess the human health impact over China in this study.

To account for the overall human health impact caused by exposures to multiple air pollutants, and to reflect the linear exposure-response relationship between air pollution and health risks, an aggregate risks index (ARI) (Cairncross et al., 2007) was adopted to assess human health risks. This index is based on the exposure-response relationship and relative risks (RR) of the increased mortality related to exposure to each individual air pollutant, and it is believed that this index can help us to understand the overall health impact of multiple air pollutants.. According to the definition of ARI, , total human health risks by exposure to several air pollutants are the sum of the risks associated with each air pollutant, and are given as (Cairncross et al., 2007):

$$ARI = \sum_{i=1}^{n} PSI_i = \sum_{i=1}^{n} a_i \times C_i \quad (1)$$

where PSI_i is defined to reflect the contribution of individual pollutant to the total health risks, n is the number of pollutants, C_i is corresponding air pollutant

concentrations, and a_i is an coefficient which is directly proportional to the incremental risk values.

Among the six air pollutants, PM_{10} concentrations could be treated as the most significant factor and therefore can be used as a predictor of mortality when calculating a_i (Pyta, 2008), i.e., a_i values were determined in terms of RR value relative to that ofPM_{10}. For each pollutant, a_i is defined as:

$$a_i = \frac{a_{PM10} \times (RR_i - 1)}{RR_{PM10} - 1} \quad (2)$$

where RR_i is the relative risk of mortality for the increase of 10 μg/m^3 in air pollution concentrations. a_{PM10} is a constant with a value of0.080, and it is determined by the health endpoints (Sicard et al., 2011). Since mortality was the most significant health endpoint to all air pollutants, it was considered as the only health endpoint in this index. The RR values of mortality for general population are adopted from previous researches (WHO, 2000; Cairncross et al., 2007), and are shown in Table 1.

Table 1: RR of mortality per 10 μg/m^3 increase in pollutant concentrations

	PM10	PM2.5	NO2	SO2	O3	CO
RR	1.0074	1.015	1.003	1.004	1.0051	1.04
(95% CI)	1.0062-1.0086	1.011-1.019	1.0018-1.0034	1.003-1.005	1.0028-1.0066	1.03-1.05

2.2.2 Satellite data collection and processing

In this study, daily OMI Level-2 Near-UV Aerosol Optical Depth-OMAERUV products (http://disc.sci.gsfc.nasa.gov/Aura/data-holdings/OMI/omaeruv_v003.shtml) over the time period of 2010 was used to estimate PM10 and PM2.5 concentrations. The products are produced at the spatial resolution of 0.125°×0.125°, and are consisted of AOD, aerosol absorption optical depth (AAOD), and single scattering albedo (SSA) at 354, 388 and 500 nm. The OMI AOD product has been validated against AERONET measurements, it is indicated that correlation coefficient between OMI AOD products and AERONET observations is in the range 0.79-0.92, and intercept is in the range 0.63-0.92 (NASA, 2012). Since the inversion in UV channel could be affected by Rayleigh scattering easily, the accuracy is relatively low in low AOD areas and the

accuracy is high in high AOD areas (Li et al., 2014; Torres et al., 2007). Therefore, OMAERUV products are the most appropriate to derive PM in China, where AOD is relatively high in most areas. Monthly average AOD is derived from the daily AOD products.

Monthly average Level-2 OMI NO_2 data products (http://disc.sci.gsfc.nasa.gov/Aura/data-holdings/OMI) contain parameters such as total troposphere NO_2 columns, slant column density, fitting root mean square (RMS). The total troposphere NO_2 columns, which were derived from satellite observations based on slant column retrievals with the differential optical absorption spectroscopy (DOAS) technique, are used in our studies to calculate ground NO_2 concentrations over the time period of 2010 in China. These data have a spatial resolution of 0.125°×0.125°, and their valid range is from 0 to 20 (10^{15} molecule/cm^2). The fitting error in the NO_2 slant column is estimated to be 0.3-1x1015 cm^{-2}, before the row anomaly (RA) (NASA, 2012; Celarier et al., 2011). The monthly average of total troposphere NO_2 columns is derived from valid daily total column by excluding missing data or bad quality data.

The ground SO_2 concentrations used in our studies for the time period of 2010 are from monthly average of the Level 2 OMI SO_2 total columns data (http://disc.sci.gsfc.nasa.gov/Aura/data-holdings/OMI). They are derived with DOAS technique with a spatial resolution of 0.125°×0.125°. The estimated noise standard deviation of SO_2 is 1.2-1.5 DU in the tropics (NASA, 2012; Yang et al., 2007).

The monthly average ground O_3 concentration is derived from daily total column ozone which is from the OMI Level 2 Total Column Ozone Product (http://disc.sci.gsfc.nasa.gov/Aura/data-holdings/OMI) over the period of 2010. It has a spatial resolution of 0.125°×0.125° and in Dobson Units. This OMI tropospheric column ozone product is also derived with DOAS fitting technique that essentially uses the OMI visible radiance values between 331.1 and 336.1 nm. The total ozone data in OMI products have a root-mean squared error of 1-2% (NASA, 2012; Yang et al., 2007).

Monthly average Level-2 SCIAMACHY CO products with the spatial resolution

of 0.125°×0.125° are used in this study to derive the ground CO concentrations (http://www.sciamachy.org/products/index.php?species=CO). This product is derived with DOAS fitting technique based on the solar spectral reflectance in the channel 8, which is set in the range of 2265 nm to 2380 nm, and with a valid range is from 0 to 10 (10^{18} molecule/cm^2). The bias of derived total columns is less than 20% (De Laat et al., 2012; http://www.sciamachy.org/validation).

2.2.3 Estimating ground level concentrations of air pollutants from remote sensing data

Estimating concentrations of PM_{10} and $PM_{2.5}$

Since ground PM_{10} concentrations are defined as the surface concentrations of the particles with a diameter less than 10 μm, while AOD retrieved from satellite observations corresponds to total column concentrations of particles with all sizes under ambient relative humidity, the direct correlation between satellite-based AOD and the ground concentrations of PM_{10} is usually relatively low. In addition, due to the hydroscopic growth of aerosols, relative humidity has to be taken into account in order to estimate accurately the ground PM_{10} concentrations from satellite observations data.

The relationship between PM_{10} and extinction coefficient under dry condition could be expressed as (Koelemeijer et al., 2006; Wang et al., 2010):

$$\sigma_{a,dry} = \frac{3Q_{ext}}{4\gamma_{eff}\rho} PM_{10} = \alpha_{ext,10} \cdot PM_{10} \quad (3)$$

where $\sigma_{a,dry}$ is the extinction coefficient under dry condition, Q_{ext} is the size-distribution integrated extinction efficiency, γ_{eff} is the effective radius, ρ is the aerosol mass density, and $\alpha_{ext,10}$ is the mass extinction efficiency of the aerosol mixtures.

The effect of humidity on light extinction was given as follows (Lin et al., 2015):

$$f(RH) = \frac{\sigma_a}{\sigma_{a,dry}} = \left(\frac{1-RH}{1-RH_0}\right)^{-\gamma} \quad (4)$$

where γ is the Hanel growth coefficient, which is dependent on the aerosol property. RH_0 is set at 40% (Lin et al., 2015), RH is the relative humidity.

196 The variation of aerosol extinction coefficient (σ_z) with the height can be
197 described as an exponential function (Lin et al., 2015):

198 $$\sigma_z = \sigma_a \times e^{-\frac{z}{H}} \quad (5)$$

199 Where H is the aerosol scaling height, and z is the height, σ_a is the extinction
200 coefficient on the ground.

201 Since AOD is an integral of aerosol extinction coefficient in the total column, we
202 could get (Wang et al., 2015):

203 $$AOD = \int_0^\infty \sigma_z \, dz = \int_0^\infty \sigma_a \times e^{-\frac{z}{H}} \, dz = H \times \sigma_a \quad (6)$$

204 Therefore, $\sigma_a = AOD/H$, where H is the aerosol scaling height.

205 Combine equation (3) (4) (5) (6), the relationship between RH and concentrations
206 of PM_{10} can be written as:

207 $$PM_{10} = \frac{1}{\alpha_{ext,10}} \cdot \frac{\sigma_a}{f(RH)} = \frac{1}{\alpha_{ext,10}} \cdot \frac{\frac{AOD}{H}}{(\frac{1-RH}{1-RH_0})^{-\gamma}} \quad (7)$$

208 where $\alpha_{ext,10}$ is the mass extinction efficiency (MEE) of mixed aerosol mixtures. γ is
209 the Hanel growth coefficient, which is depend on aerosol property, AOD is the aerosol
210 optical depth from OMI products, H is the aerosol scaling height, which was estimated
211 from 98 solar radiation observation stations in China over the time period of 2010 by
212 using Kriging interpolation. RH was obtained from 183 meteorological stations in
213 China over the time period of 2010 by using Kriging interpolation as well.

214 And the relationship between PM_{10} and $PM_{2.5}$ could be written as (Lin et al.,
215 2015) :

216 $$PM_{2.5} = F \cdot PM_{10} = \frac{\frac{AOD}{H}}{(\frac{\alpha_{ext,10}'}{F'})(\frac{1-RH}{1-RH_0})^{-\gamma'}} \quad (8)$$

217 where γ' is the integrated humidity effect, $\alpha_{ext,10}'$ is the reference mass extinction
218 efficiency of mixed aerosols and F' is the reference fine mode fraction, F is the scale
219 coefficient.

220 **Estimating concentrations of NO_2, SO_2 and CO**

221 The main sources of NO_2, SO_2 and CO are emissions from fossil fuels combustion
222 and biomass burning, therefore, NO_2, SO_2 and CO in the air are mainly distributed in
223 the troposphere and below the planetary boundary layer (PBL), and columns above the

top of PBL could be ignored (Boersma et al, 2008). Therefore, it is assumed that mixing volume ratios of both NO_2, SO_2 and CO are consistent from the ground to the top of the mixing layer, and concentrations are zero above the height of mixing layer (Boersma et al., 2009). Based on this assumption, total troposphere columns of both NO_2, SO_2 and CO are the integral of the concentrations with respect to the height (Ding et al., 2011):

$$VCD_{NO_2} = \int_0^{h_{PBL}} r_{NO2}\,\rho_a(h)dh = \int_0^{h_{PBL}} r_{NO2}\,\rho_{0a} e^{1-\frac{h}{H}} dh \quad (9)$$

$$VCD_{SO_2} = \int_0^{h_{PBL}} r_{SO2}\,\rho_a(h)dh = \int_0^{h_{PBL}} r_{SO2}\,\rho_{0a} e^{1-\frac{h}{H}} dh \quad (10)$$

$$VCD_{CO} = \int_0^{h_{PBL}} r_{CO}\,\rho_a(h)dh = \int_0^{h_{PBL}} r_{CO}\,\rho_{0a} e^{1-\frac{h}{H}} dh \quad (11)$$

where r_{NO2} and r_{SO2} are the mixing volume ratio of NO_2 and the mixing volume ratio of SO_2, VCD_{NO_2} and VCD_{SO_2} are the total NO_2 column and the total SO_2 column, ρ_a is the number density of molecules, ρ_{0a} is the air density near the ground, h_{PBL} is the height of mixing layer, and H is the aerosol scale height.

According to equation (9), equation (10) and equation (11), we could obtain the mixing volume ratio of NO_2 and SO_2 (Ding et al., 2011):

$$r_{NO2} = \frac{VCD_{NO_2}}{\rho_{0a}} \left(\frac{1}{H} + \frac{1}{h_{PBL}}\right) \quad (12)$$

$$r_{SO2} = \frac{VCD_{SO_2}}{\rho_{0a}} \left(\frac{1}{H} + \frac{1}{h_{PBL}}\right) \quad (13)$$

$$r_{CO} = \frac{VCD_{CO}}{\rho_{0a}} \left(\frac{1}{H} + \frac{1}{h_{PBL}}\right) \quad (14)$$

VCD_{NO_2}, VCD_{SO_2} and VCD_{CO} were obtained from satellite observations, h_{PBL} was obtained from 98 solar radiation observation stations in China over the time period of 2010 by using Kriging interpolation. H is the aerosol scaling height, which is defined as the height at which the aerosol extinction coefficient is reduced to 1/e of the ground value. It is considered as the equivalent depth of the optically active aerosol layer of the atmosphere and could be approximated by the boundary layer height (Koelemeijer et al., 2006). The spatial distribution of monthly average temperature was from 183 meteorological stations in China by using Kriging interpolation, and then ρ_{0a} was calculated according to the relationship between air density and temperature (Bartman et al., 1956). According to equation (12), equation (13) and equation (14), we obtained the surface mixing volume ratio of NO_2, SO_2 and CO, then we could convert the units

of NO_2, SO_2 and CO from mixing volume ratio to mass concentrations easily.

Estimating concentrations of O_3

Retrieval of ground O_3 from satellite remote sensing remains a difficult task. To get ground mass concentrations of O_3, the column density was firstly converted to number density according to equation (15) (Sheng-bo et al., 2010):

$$N_h = \int_0^h n_i \, dh \tag{15}$$

where N is the column density, n_i is the number density of molecules, h represents the height, h_i is the height of i-th layer.

According to equation (15), we could obtain:

$$N_{h_{i-1}} - N_{h_i} = \int_{h_{i-1}}^{h_i} n_i dh = \overline{n_{i-1}} h_{i-1} \tag{16}$$

According to the definition of Dobson Units (University of Cambridge, 2010):

$$VCD_{O_3} = \frac{V}{S} = \frac{N}{N_A} V_m \tag{17}$$

where N_A is the Avogadro's number, and V_m is the molar volume of gas, VCD_{O_3} is the columns that from satellite observations.

According to equation (16) and equation (17) (Sheng-bo et al., 2010):

$$n_{i-1} = \frac{N_A VCD_{O_3}}{V_m h_{i-1}} \tag{18}$$

Finally, we could obtain the surface number density of molecules, and could convert the units of O_3 from number density to mass concentrations.

3 Results

3.1 Spatial distribution of air pollutants in China

Spatial distribution of PM_{10} in China

The PM_{10} spatial distribution in 2010 is derived from Equation (7), and is given in Fig. 1. The spatial resolution of the map is 0.125°×0.125°. It is seen that the highest PM_{10} concentrations, with an average PM_{10} concentration greater than 85 μg/m^3, are located at Northern China and the Sichuan Basin as a result of heavy industry. In the middle and lower reaches of Yangtze River, Inner Mongolia, Shaanxi, Shanxi and some

provinces in north China, PM_{10} concentrations are about 70 μg/m^3. The lowest PM_{10} concentrations appeared over Tibetan Plateau, Fujian and Heilongjiang, due to the fact that there is less human destruction of the nature environments in Tibet, and forest coverage rates are higher in Heilongjiang and Fujian.

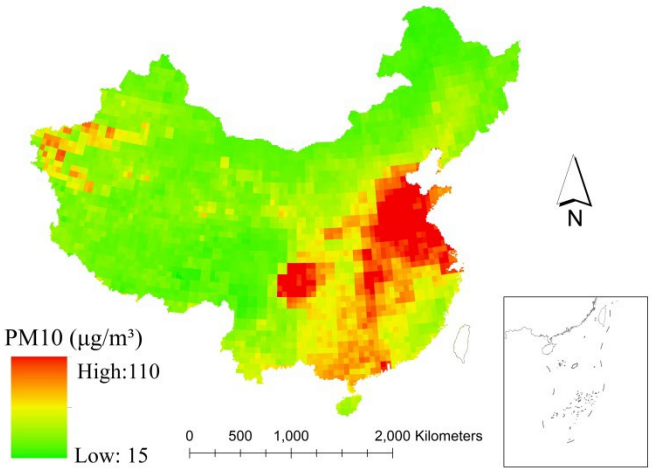

Fig. 1. Spatial distribution of PM_{10} in China in 2010

Spatial distribution of $PM_{2.5}$ in China

Since $PM_{2.5}$ concentrations are well correlated with concentrations of PM_{10}, the spatial distribution of $PM_{2.5}$ shows similar patter as the distribution of PM_{10}, as given in Fig. 2. The spatial resolution of this map is also 0.125°×0.125°. In general, the worst places for $PM_{2.5}$ pollution are also in Northern China and Sichuan Basin, and the annual average $PM_{2.5}$ concentrations can exceed 65 μg/m3. This is consistent with the fact that the heavy industry is concentrated in these two regions. It is also seen that the high $PM_{2.5}$ pollution appears in lower reaches of Yangtze River and southern China, where are the numerous mega-cities and fast expansions located. The lowest $PM_{2.5}$ concentrations in 2010, with average concentrations about 15 μg/m3, are located in Tibetan Plateau due to their pristine environment.

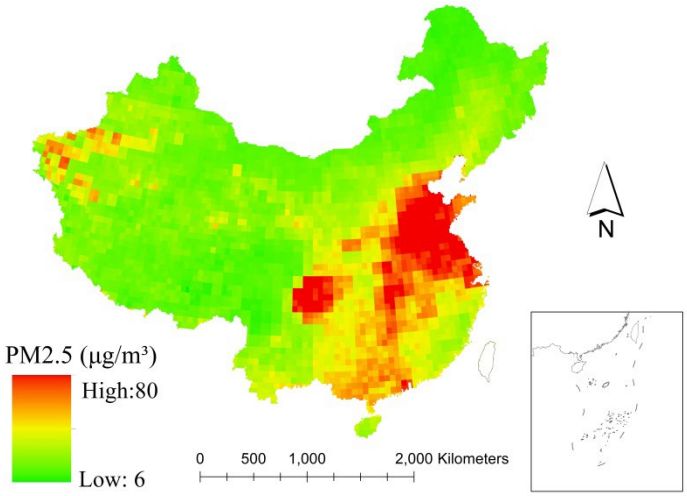

Fig. 2. Spatial distribution of $PM_{2.5}$ in China in 2010

Spatial distribution of NO_2 in China

The main sources of troposphere NO_2 are emissions from fossil fuels combustion and biomass burning, and the vehicle exhaust emissions also account for a large proportion of the total emissions (Liang et al. 1998). Fig. 3 is the spatial distribution of NO_2 in China in 2010 with a resolution of 0.125° ×0.125° . As shown in Fig. 3, NO_2 pollution is more serious over large cities. The most polluted cities, with average NO_2 concentrations about 45 μg/m^3 in 2010, are mainly located in large cities over Northern and Eastern China, such as Shenyang, Chongqing, where many heavy industries are located, and Beijing, Tianjin, Shanghai, Guangzhou, where the number of vehicles is large and expanding. NO_2 pollution is much less in western and southern regions of China, especially in mountainous and plateau areas.

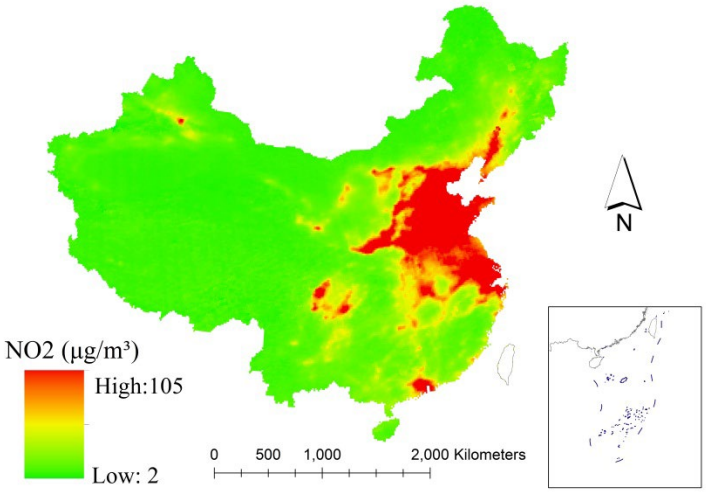

Fig. 3. Spatial distribution of NO_2 in China in 2010

Spatial distribution of SO_2 in China

Coal combustion in industrial facilities and power plants has become the main sources of SO_2 emissions in China (Henriksson et al. 2011). According to equation (13), we obtained the spatial distribution of SO_2 in China with a resolution of 0.125° ×0.125° , as shown in Fig. 4. The heavy industries are mainly located in Northern China and Northeastern China, therefore, the SO_2 pollution is most serious in these areas, where the concentrations can exceed 50 μg/m^3. In southern China, such as Fujian, Guangdong, Guangxi and Yunnan, SO_2 concentrations are relatively lower, with a value of about 25 μg/m^3. In Western regions, such as Xinjiang, Tibetan Plateau, average SO_2 concentrations are less than 10μg/m^3 due to less SO_2 pollution sources.

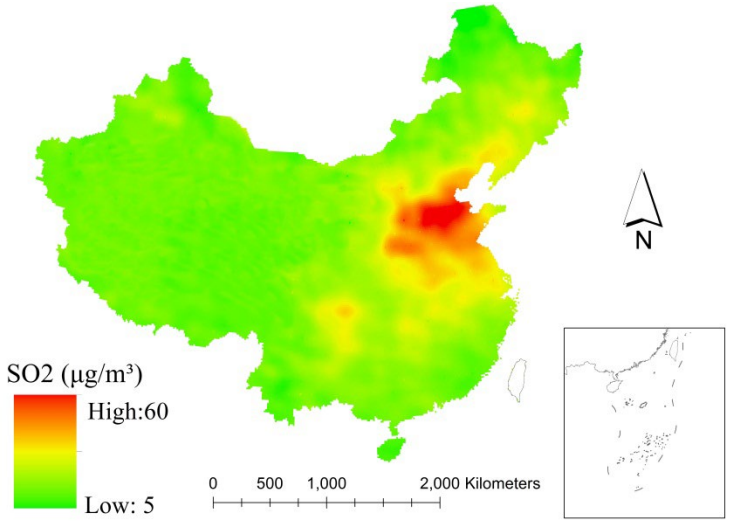

Fig. 4. Spatial distribution of SO_2 in China in 2010

Spatial distribution of O_3 in China

According to equation (18), we obtained the spatial distribution of O_3 in China with a resolution of 0.125° ×0.125° , as shown in Fig. 5. The O_3 concentrations generally follow latitude distribution, i.e., increase with the increasing latitude in China. The highest O_3 concentrations are mainly concentrated in Northeastern China, where the average O_3 concentrations are about 60 μg/m^3. It is indicated that the Tibetan Plateau and its surrounding regions show relative lower values of O_3 concentrations, about 25

μg/m^3. The topography features and thermal effects are the main reasons for low O_3 concentrations over Tibetan Plateau (Zou, 1996).Due to the influence of the Mongolian High and Aleutian Low, high ozone horizontal fluxes transport along the Mongolia and Northeastern China, which cause the highest concentration of ozone in Northeastern China (Ma et al., 2002; Jie et al., 2009). Ozone is related to photochemical reactions, and also the emission levels of NOx and VOCs. Although the net ozone photochemical production in Northern and Eastern China is high, ozone could not accumulate due to the effects of East Asian Monsoon (Jie et al., 2009).

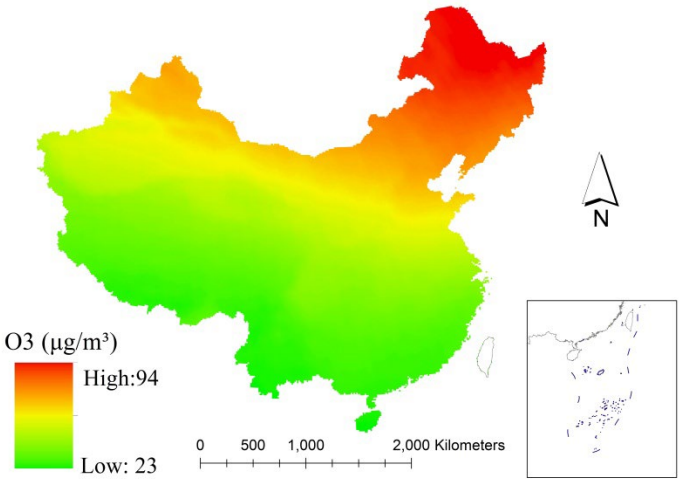

Fig. 5. Spatial distribution of O_3 in China in 2010

Spatial distribution of CO in China

The main sources of CO in the troposphere are the burning of biomass burning (Novelli et al., 1994). Therefore, the distribution of CO is highly consistent with the distribution of industrial areas and cities. The spatial distribution of CO in China with a resolution of 0.125° ×0.125° is shown in Figure 6. In China, the high concentrations of CO mainly distributed in Northern China and Sichuan Basin, in which many big cities and industries districts located, and the average concentrations of CO in 2010 are about 25μg/m^3. The lowest CO concentrations in 2010, with average concentrations less than 10 μg/m^3, are located in Tibetan Plateau. This is because the number of manmade emissions is less.

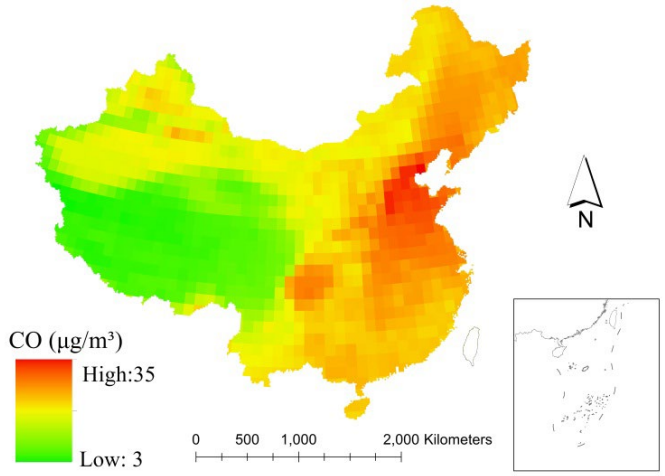

Fig. 6. Spatial distribution of CO in China in 2010

3.2 Aggregate human health risks in China

To account for the human health impact from the exposure to multiple air pollutants, we adopted an aggregate risks index in this paper, and obtained the spatial distribution of ARI values in China, which is shown in Fig. 7. According to the classification standard of the ARI values (Sicard et al., 2011), it is considered as the highest health risks when the ARI values exceed 10. It is seen that areas with the highest risks are mainly located in Northern China and Sichuan Basin, where PM_{10}, $PM_{2.5}$, NO_2, SO_2 pollution is all very serious. In Central and Southern China, the ARI values are between 7 and 9, indicating very high human health risks in these areas. This mainly caused by the large number of cities and industries, which results in a large number of vehicles and a high population density in these areas. In Tibetan Plateau, the ARI values are the lowest, less than 5, i.e., air pollution has the lowest impact on human health in these regions.

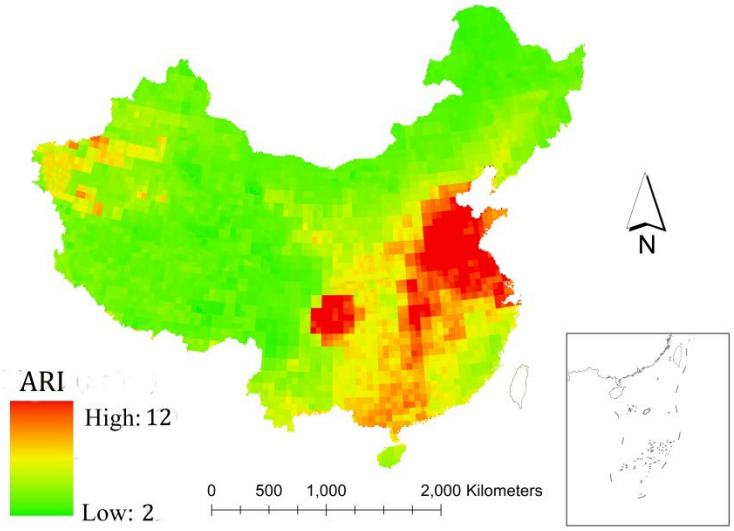

Fig. 7. Spatial distribution of ARI in China in 2010

4 Discussion

4.1 Validation of satellite-derived air pollution concentrations

The precision and accuracy of satellite-derived air pollutant concentrations determines the uncertainties in estimation of the human health impact from air pollution. To estimate the accuracy of the satellite derived air pollutant concentrations, the measured average PM_{10}, NO_2 and SO_2 concentrations in 138 Chinese cities, the average CO concentrations in 23 Chinese cities, and the average O_3 concentrations in 12 Chinese cities in 2010 were collected as truth data. Note that, air pollutant concentrations in each city were the mean value of all the monitoring stations in both urban and suburban areas. However, since $PM_{2.5}$ and O_3 concentrations were not included in the air quality standard in China until February 2012, the measured of ground-level O_3 concentrations are only available in 12 pilot cities, but no surface measurement $PM_{2.5}$ concentrations are available in 2010. Therefore, validations are only carried out for PM_{10}, NO_2, SO_2, CO and O_3. Since satellite data are processed on a monthly basis, validation of monthly average satellite derived air pollutants concentrations was carried out, as shown from Table 2 to Table 6. In general, a good agreement exists between the ground measured monthly average concentrations of each pollutant and satellite derived monthly average concentrations, with a very low root mean square error (RMSE) and relative error (RE).

Table 2 Comparison of ground measured monthly average PM_{10} and satellite derived monthly average PM_{10}

	Jan	Feb	Mar	Apr	May	Jun	Jul	Aug	Sep	Oct	Nov	Dec
R2	0.52	0.62	0.69	0.74	0.72	0.76	0.79	0.71	0.65	0.62	0.58	0.64
RMSE	10.78	10.21	9.25	8.46	7.25	7.55	7.69	8.56	7.84	8.33	9.14	7.42
RE(%)	11.2	10.78	12.14	9.33	8.90	8.12	7.59	9.21	10.69	11.26	10.79	9.41

Table 3 Comparison of ground measured monthly average NO_2 and satellite derived monthly average NO_2

	Jan	Feb	Mar	Apr	May	Jun	Jul	Aug	Sep	Oct	Nov	Dec
R2	0.49	0.52	0.54	0.51	0.68	0.71	0.76	0.56	0.70	0.58	0.60	0.44
RMSE	13.77	11.39	11.56	11.73	10.20	9.86	8.30	10.92	9.94	10.65	11.20	12.69
RE(%)	11.59	11.04	10.88	10.85	10.54	9.33	8.67	10.31	9.52	10.22	9.92	12.10

Table 4 Comparison of ground measured monthly average SO_2 and satellite derived monthly average SO_2

	Jan	Feb	Mar	Apr	May	Jun	Jul	Aug	Sep	Oct	Nov	Dec
R2	0.55	0.60	0.61	0.58	0.69	0.75	0.76	0.64	0.62	0.56	0.63	0.57
RMSE	9.21	8.67	8.03	9.56	7.80	6.65	6.93	7.97	8.21	10.61	8.30	10.64
RE(%)	12.92	11.78	11.60	10.24	9.57	8.33	8.52	9.62	9.50	11.38	10.87	11.05

Table 5 Comparison of ground measured monthly average O_3 and satellite derived monthly average O_3

	Jan	Feb	Mar	Apr	May	Jun	Jul	Aug	Sep	Oct	Nov	Dec
R2	0.52	0.50	0.60	0.66	0.70	0.72	0.77	0.69	0.64	0.71	0.73	0.63
RMSE	12.45	12.50	10.89	11.65	10.78	9.46	8.53	10.58	10.97	11.21	8.90	11.15
RE(%)	13.86	10.63	11.40	11.05	9.65	9.28	8.67	9.90	10.32	9.98	10.62	11.33

Table 6 Comparison of ground measured monthly average CO and satellite derived monthly average CO

	Jan	Feb	Mar	Apr	May	Jun	Jul	Aug	Sep	Oct	Nov	Dec
R2	0.51	0.49	0.60	0.62	0.62	0.69	0.70	0.68	0.64	0.59	0.61	0.63
RMSE	9.14	12.50	9.89	9.77	11.53	8.84	8.75	9.10	10.55	9.37	10.02	9.64
RE(%)	14.24	12.35	10.87	11.32	10.98	9.31	8.53	8.80	9.25	11.33	10.48	12.67

Validation of annual average satellite derived air pollutants concentrations is given in Figure 8. In general, a good liner relationship exists between satellite-derived air pollutant concentrations and ground-based concentrations. The correlation coefficient between surface measurement PM_{10}, NO_2, SO_2, O_3, CO concentrations and

412 corresponding satellite derived concentrations can be as high as 0.71, 0.65, 0.79, 0.72
413 and 0.67 respectively. The root mean square error (RMSE) is about 8.31, 12.77, 7.94,
414 10.23 and 9.45, and the average relative error (RE) is about9.32%, 12.33%, 9.76%,
415 11.56% and 10.50%, respectively. High correlation and low estimated standard error
416 indicates the applicability and reliability of air pollutant concentrations derived from
417 satellite observations. The bias of satellite derived concentrations of PM_{10}, NO_2, SO_2,
418 O_3 and CO is about 11 μg/m^3, 9 μg/m^3, 9 μg/m^3, 7 μg/m^3, 11 μg/m^3, respectively.
419 According to the rule of transferred bias, bias of $PM_{2.5}$ could be written as :

420 $$m_{PM2.5} = k \cdot m_{PM10} \quad (19)$$

421 where $m_{PM2.5}$, m_{PM10} is the bias of satellite derived $PM_{2.5}$ and PM_{10}, k is the scale
422 coefficient which could be defined by the relationship between PM_{10} and $PM_{2.5}$ in
423 Equation (8) . And we could obtain the transferred bias for $PM_{2.5}$, is about 15μg/m^3,
424 and the overall bias for ARI values is estimated to be about 1.0.
425

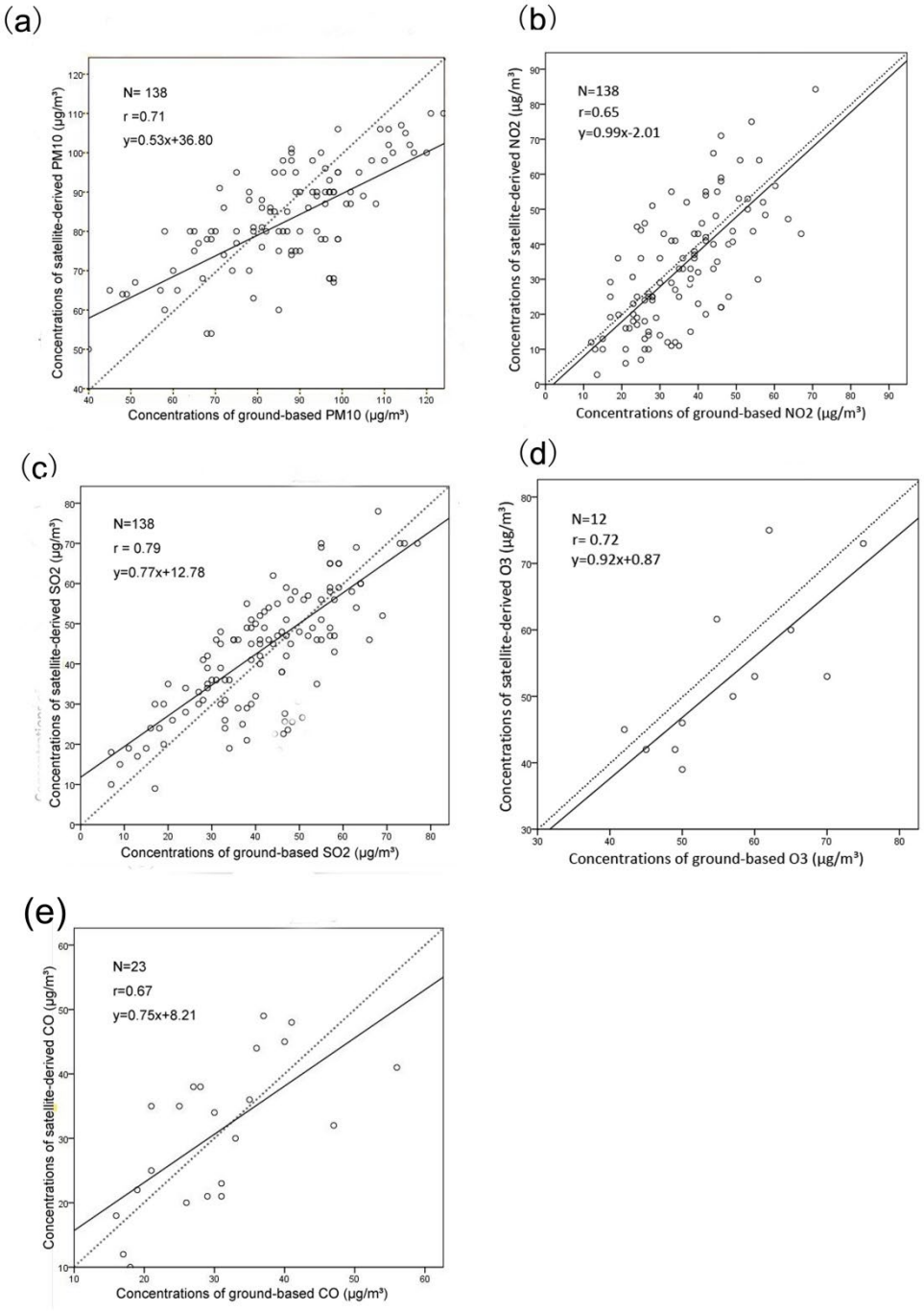

Fig.8. Comparison of ground based air pollutant concentrations and satellite derived air pollutant concentrations

4.2 Advantages of satellite observations in estimating human health impact

The human health impact caused by air pollution is usually over-estimated by using the in-situ air pollution data (Wilson et al., 1997; Brauer et al., 2003), since air monitoring stations are mainly located in the areas where concentrations of air pollutants are generally higher. By using the ground based monitoring data to represent

the concentrations in the whole region, human health impact is most likely overestimated. Although some interpolation methods are applied to the ground-based observation of air pollution in the human health impact assessment, the interpolation methods are constrained by physiochemical models, and the accuracy is not satisfactory (Hertel et al., 2001). In our study, concentrations of air pollutants were all derived from satellite observations data, which could provide much better spatial coverage. By analyzing the distribution of air pollutants and corresponding human health impact, the spatial distribution of ARI values were obtained and were used to measure aggregate human health risks.

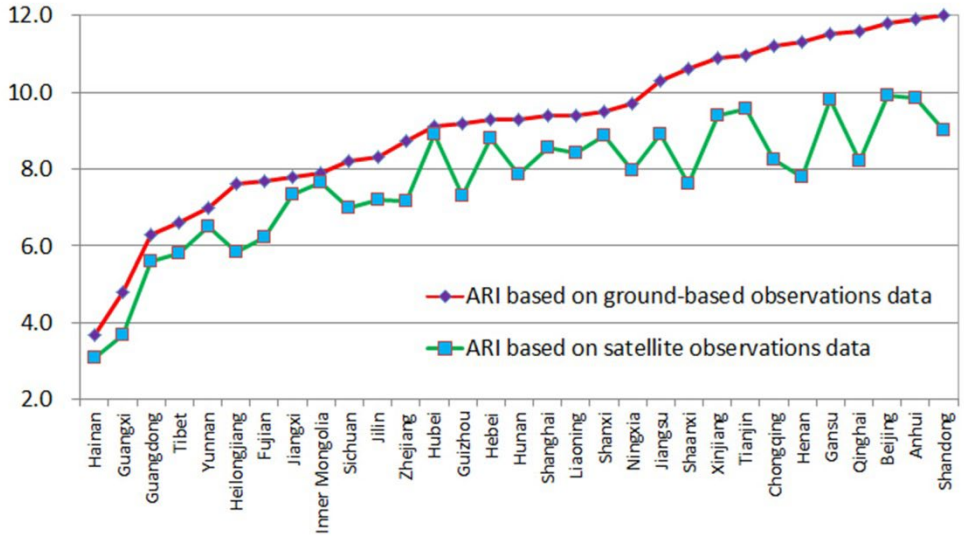

Fig. 9. Comparison of ARI values based on in-situ data with that based on satellite observations data at a provincial scale

Compared with the assessment based on in-situ air pollution data, the human health risks based on satellite observations data are apparently lower, as shown in Fig. 9. We found that the ARI values based on satellite observations data are all lower than those based on in-situ data at a provincial scale. According to the results based on in-situ data, average ARI values are greater than 10 in eleven provinces, which mean human health risks are extremely high. While average ARI values are all lower than 10 when using the satellite observations data. That indicates human health risks based on in situ measurements alone may lead to extravagate human health impact by air pollutants. Air monitor stations are mainly clustered in areas of poor air quality. The in-situ

observations are spatially less representative, while satellite observations provide better spatial coverage. Therefore, human health risks assessment based on remote sensing data is more suitable.

Single pollutant analysis of health impact is inadequate to reflect the overall air pollution damages to human health (Brauer et al., 2003; Chen et al., 2005). The human health impact of air pollution is caused by the exposure to multiple air pollutants, therefore, the major contributors to the health problems should be all considered. In our research, we linked air pollution and outcomes of human mortality using an aggregate risks index. The aggregate risks index has been proven to be an effective way to integrate the human health impact of all air pollutants, and to determine the contribution of each air pollutant to human health (Chen et al., 2013).

5 Conclusion

In this paper, the overall human health impact caused by exposure to multiple air pollutants in China was accessed based on data derived from satellite observations. First of all, concentrations of ground PM_{10}, $PM_{2.5}$, SO_2, NO_2 and O_3 were derived from the corresponding OMI Lever 2 product, and concentrations of ground CO were derived from SCIAMACHY data in this paper. Secondly, to study the relative contribution of each air pollutant to human health risks, a novel index (ARI) was adopted to assess the aggregated human health risks in China related to multiple air pollutants. Finally, the spatial distribution of human health risks in China was obtained by analyzing the distribution of concentration of each air pollutant and corresponding relative risks of mortality. It is found that human health impact accessed with satellite observations is generally lower than that obtained from in-situ data. In addition, it is indicated that remote sensing observations have advantages over in-situ data in accessing human health impact caused by air pollution, as a result of better spatial coverage, therefore, better understanding of the spatial distribution of human heath impact. As for China, areas with the highest risks caused by air pollution are mainly located in Taklimakan Desert regions, Northern China, Sichuan Basin and the middle of Inner Mongolia. Followed by Northeastern and Southern China, very high

human health risks exist in these areas. In Tibetan Plateau and some mountainous areas over central China, air pollution has the lowest impact on human health.

Studies on the human health impact caused by exposure to air pollutants are important in environmental damages assessment, as well as in health insurance industry. However, assessing the human health impact accurately by exposure to multiple air pollutants is comprehensive and complex. In this study, the impact caused by the combined contamination of several air pollutants is not discussed. In addition, how to combine air pollution monitoring stations data with emissions data, and integrate the corresponding health impact will be another challenge, which may be tackled in the future. Finally, it should be noted that remote sensing data can only monitor outdoor air pollution, thus, the methods proposed in this paper are not suitable for assessing human health impact caused by indoor air pollution.

Acknowledgements

This study was supported by Major Program of National Social Science Foundation of China (11&ZD157). Thanks for Pingping Yao and Xi Yang's work in data collection and processing in the first revision. Thanks for the reviewer's constructive comments and insightful suggestions.

References

Anderson, J. O., Thundiyil, J. G., & Stolbach, A. (2012). Clearing the air: a review of the effects of particulate matter air pollution on human health. *Journal of Medical Toxicology, 8*(2), 166-175.

Balis, D., Kroon, M., Koukouli, M. E., Brinksma, E. J., Labow, G., Veefkind, J. P., & McPeters, R. D. (2007). Validation of Ozone Monitoring Instrument total ozone column measurements using Brewer and Dobson spectrophotometer ground-based observations. *Journal of Geophysical Research: Atmospheres, 112*, D24S46.

514 Bartman, F. L., Chaney, L. W., Jones, L. M., & Liu, V. C. (1956). Upper‐Air Density
515 and Temperature by the Falling-Sphere Method. *Journal of Applied Physics, 27*(7),
516 706-712.

517 Bernstein, J. A., Alexis, N., Barnes, C., Bernstein, I. L., Nel, A., Peden, D., ... &
518 Williams, P. B. (2004). Health effects of air pollution. *Journal of Allergy and*
519 *Clinical Immunology*, *114(5)*, 1116-1123.

520 Boersma, K. F., Jacob, D. J., Bucsela, E. J., Perring, A. E., Dirksen, R., Van Der A, R.
521 J., ... & Cohen, R. C. (2008). Validation of OMI tropospheric NO_2 observations
522 during INTEX-B and application to constrain NO_x emissions over the eastern
523 United States and Mexico. *Atmospheric Environment, 42*(19), 4480-4497.

524 Boersma, K. F., Jacob, D. J., Trainic, M., Rudich, Y., DeSmedt, I., Dirksen, R., & Eskes,
525 H. J. (2009). Validation of urban NO_2 concentrations and their diurnal and
526 seasonal variations observed from the SCIAMACHY and OMI sensors using in
527 situ surface measurements in Israeli cities. *Atmospheric Chemistry and*
528 *Physics, 9(12),* 3867-3879.

529 Brauer, M., Hoek, G., van Vliet, P., Meliefste, K., Fischer, P., Gehring, U., ... &
530 Brunekreef, B. (2003). Estimating long-term average particulate air pollution
531 concentrations: application of traffic indicators and geographic information
532 systems. *Epidemiology, 14*(2), 228-239.

533 Cairncross, E. K., John, J., & Zunckel, M. (2007). A novel air pollution index based on
534 the relative risk of daily mortality associated with short-term exposure to common
535 air pollutants. *Atmospheric Environment, 41*(38), 8442-8454.

536 Campbell, J. B. (2002). Introduction to Remote Sensing. *Boca Raton: CR*C Press.

537 Celarier, E. A., Lamsal, L., Krotkov, N. A., Bucsela, E. J., Herman, J. R., Dickerson, R.
538 R., ... & Gleason, J. F. (2011, December). Evaluation of improved operational
539 standard tropospheric NO_2 retrievals from Ozone Monitoring Instrument using in
540 situ and surface-based NO_2 observations. InAGU Fall Meeting Abstracts (Vol. 1, p.
541 0360).Chan, C. K., & Yao, X. (2008). Air pollution in mega cities in China.
542 *Atmospheric Environment, 42*(1), 1-42.

543 Chen, B., Hong, C., & Kan, H. (2004). Exposures and health outcomes from outdoor air
544 pollutants in China. *Toxicology, 198*(1), 291-300.

545 Chen, L. H., Knutsen, S. F., Shavlik, D., Beeson, W. L., Petersen, F., Ghamsary, M., et
546 al. (2005). The association between fatal coronary heart disease and ambient
547 particulate air pollution: are females at greater risk? *Environmental Health*
548 *Perspectives, 113*(12), 1723–1729.

549 Chen, R., Huang, W., Wong, C. M., Wang, Z., Thach, T. Q., Chen, B., ... & CAPES
550 Collaborative Group. (2012). Short-term exposure to sulfur dioxide and daily
551 mortality in 17 Chinese cities: The China air pollution and health effects study
552 (CAPES). *Environmental Research, 118*, 101-106.

553 Chen, R., Wang, X., Meng, X., Hua, J., Zhou, Z., Chen, B., & Kan, H. (2013).
554 Communicating air pollution-related health risks to the public: an application of
555 the Air Quality Health Index in Shanghai, China. *Environment International,51*,
556 168-173.

557 De Laat, A. T. J., Dijkstra, R., Schrijver, H., Nédélec, P., & Aben, I. (2012). Validation
558 of six years of SCIAMACHY carbon monoxide observations using MOZAIC CO
559 profile measurements. *Atmospheric Measurement Techniques,5*(9), 2133-2142.

560 Dergham, M., Lepers, C., Verdin, A., Cazier, F., Billet, S., Courcot, D., ... & Garçon, G.
561 (2015). Temporal–spatial variations of the physicochemical characteristics of air
562 pollution Particulate Matter ($PM_{2.5-0.3}$) and toxicological effects in human
563 bronchial epithelial cells (BEAS-2B).*Environmental Research, 137*, 256-267.

564 Ding,Y.,Peng, L.,Ran, L., & Zhao, C. (2011). A Method of Inferring Ground Level NO2
565 Using Satellite-Borne OMI Observations. *Acta Scientiarum Naturalium*
566 *Universitatis Pekinensis, 47*(4), 671-676

567 Ding, Z., Liu, T., Rutter, N. W., Yu, Z., Guo, Z., & Zhu, R. (1995). Ice-volume forcing
568 of East Asian winter monsoon variations in the past 800,000 years. *Quaternary*
569 *Research, 44*(2), 149-159.

570 Henriksson, S. V., Laaksonen, A., Kerminen, V. M., Räisänen, P., Järvinen, H.,
571 Sundström, A. M., & Leeuw, G. D. (2011). Spatial distributions and seasonal
572 cycles of aerosols in India and China seen in global climate-aerosol
573 model. *Atmospheric Chemistry and Physics, 11*(15), 7975-7990.

574 Hertel, O., De Leeuw, F. A., Jensen, S. S., Gee, D., Herbarth, O., Pryor, S., ... & Olsen,
575 E. (2001). Human exposure to outdoor air pollution (IUPAC technical
576 report). *Pure and Applied Chemistry, 73*(6), 933-958.

577 Janssen, N. A., Schwartz, J., Zanobetti, A., & Suh, H. H. (2002). Air conditioning and
578 source-specific particles as modifiers of the effect of PM_{10} on hospital admissions
579 for heart and lung disease. *Environmental Health Perspectives, 110*(1), 43.

580 Jerrett, M., Burnett, R. T., Ma, R., Pope III, C. A., Krewski, D., Newbold, K. B., ... &
581 Thun, M. J. (2005). Spatial analysis of air pollution and mortality in Los
582 Angeles. *Epidemiology, 16*(6), 727-736.

583 Jerrett, M., Burnett, R. T., Pope III, C. A., Ito, K., Thurston, G., Krewski, D., ... & Thun,
584 M. (2009). Long-term ozone exposure and mortality. *New England Journal of*
585 *Medicine, 360*(11), 1085-1095.

586 Jie, L., Qizhong, W., & Chao, G. (2009). Model study of ozone in the boundary layer
587 over East Asia in Spring. *Research of Environmental Sciences, 22*(1), 1-6.

588 Kan, H., Wong, C. M., Vichit-Vadakan, N., & Qian, Z. (2010). Short-term association
589 between sulfur dioxide and daily mortality: the Public Health and Air Pollution in
590 Asia (PAPA) study. *Environmental Research, 110*(3), 258-264.

591 Koelemeijer, R. B. A., Homan, C. D., & Matthijsen, J. (2006). Comparison of spatial

592 and temporal variations of aerosol optical thickness and particulate matter over
593 Europe. *Atmospheric Environment, 40*(27), 5304-5315.

594 Li, L., Shi, R., Zhang, L., Zhang, J., & Gao, W. (2014, October). The data fusion of
595 aerosol optical thickness using universal kriging and stepwise regression in East
596 China. In SPIE Optical Engineering+Applications. International Society for
597 Optics and Photonics.

598 Liang, J., Horowitz, L. W., Jacob, D. J., Wang, Y., Fiore, A. M., Logan, J. A., ... &
599 Munger, J. W. (1998). Seasonal budgets of reactive nitrogen species and ozone
600 over the United States, and export fluxes to the global atmosphere. *Journal of*
601 *Geophysical Research: Atmospheres (1984–2012),103*(D11), 13435-13450.

602 Lin, C., Li, Y., Yuan, Z., Lau, A. K., Li, C., & Fung, J. C. (2015). Using satellite remote
603 sensing data to estimate the high-resolution distribution of ground-level
604 $PM_{2.5}$. *Remote Sensing of Environment, 156*, 117-128.

605 Lipsett, M. J., Ostro, B. D., Reynolds, P., Goldberg, D., Hertz, A., Jerrett, M., ... &
606 Bernstein, L. (2011). Long-term exposure to air pollution and cardiorespiratory
607 disease in the California teachers study cohort. *American Journal of Respiratory*
608 *and Critical Care Medicine, 184*(7), 828-835.

609 Ma, J., Liu, H., & Hauglustaine, D. (2002). Summertime tropospheric ozone over
610 China simulated with a regional chemical transport model 1. Model description
611 and evaluation. *Journal of Geophysical Research: Atmospheres*
612 *(1984–2012)*, *107*(D22), 27.

613 Murray, C. J., Vos, T., Lozano, R., Naghavi, M., Flaxman, A. D., Michaud, C., ... &
614 Bridgett, L. (2013). Disability-adjusted life years (DALYs) for 291 diseases and
615 injuries in 21 regions, 1990–2010: a systematic analysis for the Global Burden of
616 Disease Study 2010. *The Lancet, 380*(9859), 2197-2223.

617 NASA. (2012). Ozone Monitoring Instrument (OMI) Data User's Guide.

618 Novelli, P. C., Masarie, K. A., Tans, P. P., & Lang, P. M. (1994). Recent changes in
619 atmospheric carbon monoxide. *Science-AAAS-Weekly Paper Edition-including*
620 *Guide to Scientific Information*, *263*(5153), 1587-1589.

621 Putaud, J. P., Van Dingenen, R., Alastuey, A., Bauer, H., Birmili, W., Cyrys, J., ... &
622 Raes, F. (2010). A European aerosol phenomenology–3: Physical and chemical
623 characteristics of particulate matter from 60 rural, urban, and kerbside sites across
624 Europe. *Atmospheric Environment, 44*(10), 1308-1320.

625 Pyta, H. (2008). Classification of air quality based on factors of relative risk of
626 mortality increase. *Environment Protection Engineering, 34*(4), 111-117.

627 Raaschou-Nielsen, O., Andersen, Z. J., Beelen, R., Samoli, E., Stafoggia, M.,
628 Weinmayr, G., ... & Cesaroni, G. (2013). Air pollution and lung cancer incidence
629 in 17 European cohorts: prospective analyses from the European Study of Cohorts
630 for Air Pollution Effects (ESCAPE). *The Lancet Oncology,14*(9), 813-822.

631 Raub, J. A., Mathieu-Nolf, M., Hampson, N. B., & Thom, S. R. (2000). Carbon
632 monoxide poisoning—a public health perspective. *Toxicology*,*145*(1), 1-14.

633 Shang, Y., Sun, Z., Cao, J., Wang, X., Zhong, L., Bi, X., ... & Huang, W. (2013).
634 Systematic review of Chinese studies of short-term exposure to air pollution and
635 daily mortality. *Environment International*, *54*, 100-111.

636 Sheng-bo, W. Z. J. C., & Nian-long, L. H. H. (2010). Conversion on different
637 dimensions of atmospheric ozone. *Journal of Meteorology and Environment*,*2*,
638 12.

639 Sicard, P., Lesne, O., Alexandre, N., Mangin, A., & Collomp, R. (2011). Air quality
640 trends and potential health effects–development of an aggregate risk
641 index. *Atmospheric Environment, 45*(5), 1145-1153.

642 Smith, K. R., Jerrett, M., Anderson, H. R., Burnett, R. T., Stone, V., Derwent, R., ... &
643 Thurston, G. (2010). Public health benefits of strategies to reduce greenhouse-gas
644 emissions: health implications of short-lived greenhouse pollutants. *The*
645 *Lancet, 374*(9707), 2091-2103.

646 Torres, O., Tanskanen, A., Veihelmann, B., Ahn, C., Braak, R., Bhartia, P. K., ... &
647 Levelt, P. (2007). Aerosols and surface UV products from Ozone Monitoring
648 Instrument observations: An overview. *Journal of Geophysical Research:*
649 *Atmospheres (1984–2012), 112*(D24).

650 Turner, M. C., Krewski, D., Pope III, C. A., Chen, Y., Gapstur, S. M., & Thun, M. J.
651 (2011). Long-term ambient fine particulate matter air pollution and lung cancer in
652 a large cohort of never-smokers. *American Journal of Respiratory and Critical*
653 *Care Medicine, 184*(12), 1374-1381.

654 University of Cambridge. Dobson unit-definition. 2010.
655 http://www.atm.ch.cam.ac.uk/tour/dobson.html.

656 Wang, W., Yu, T., Ciren, P., & Jiang, P. (2015). Assessment of human health impact
657 from PM10 exposure in China based on satellite observations.*Journal of Applied*
658 *Remote Sensing, 9(1),* 096027-096027.

659 Wang, X., Lu, W., Wang, W., & Leung, A. Y. (2003). A study of ozone variation trend
660 within area of affecting human health in Hong Kong.*Chemosphere, 52*(9),
661 1405-1410.

662 Wang, Z., Chen, L., Tao, J., Zhang, Y., & Su, L. (2010). Satellite-based estimation of
663 regional particulate matter (PM) in Beijing using vertical and RH correcting
664 method. *Remote Sensing of Environment, 114*(1), 50–63.

665 Wheeler, A. J., Smith-Doiron, M., Xu, X., Gilbert, N. L., & Brook, J. R. (2008).
666 Intra-urban variability of air pollution in Windsor, Ontario—measurement and
667 modeling for human exposure assessment. *Environmental Research, 106*(1), 7-16.

668 Wilson, W. E., & Suh, H. H. (1997). Fine particles and coarse particles: concentration

669 relationships relevant to epidemiologic studies. *Journal of the Air & Waste*
670 *Management Association, 47(12)*, 1238-1249.

671 World Health Organization. (2000). Air quality guidelines for Europe. *Geneva: World*
672 *Health Organization.*

673 World Health Organization. (2005). WHO Air Quality Guidelines Global Update 2005:
674 Report on a Working Group Meeting. *Germany: WHO Regional Office for*
675 *Europe.*

676 Yang, K., Krotkov, N. A., Krueger, A. J., Carn, S. A., Bhartia, P. K., & Levelt, P. F.
677 (2007). Retrieval of large volcanic SO2 columns from the Aura Ozone Monitoring
678 Instrument: Comparison and limitations. *Journal of Geophysical Research:*
679 *Atmospheres, 112*, D24S43.

680 Zhang, Q., & Crooks, R. (2013). *Toward an Environmentally Sustainable Future:*
681 *Country Environmental Analysis of the Peoples Republic of China*. Asian
682 Development Bank.

683 Zou, H. (1996). Seasonal variation and trends of TOMS ozone over Tibet. *Geophysical*
684 *Research Letters, 23*(9), 1029-1032.